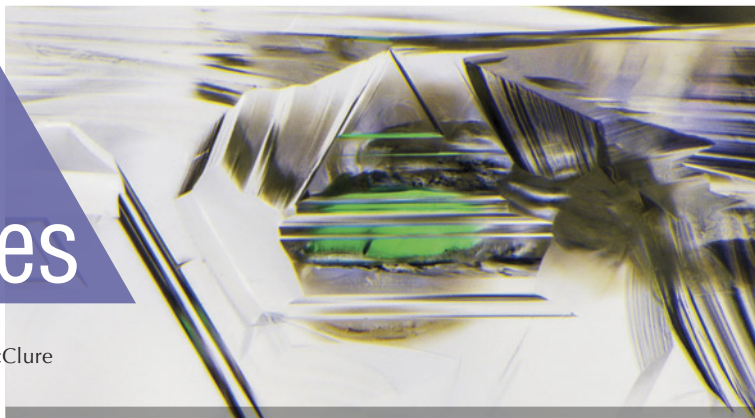


Lab Notes

Editors

Thomas M. Moses | Shane F. McClure



Rare Orange BENITOITE

A bright orange benitoite (figure 1) weighing 2.29 ct was recently examined at the Carlsbad laboratory. Standard gemological testing revealed a refractive index of 1.756 to over the limit (OTL) and a specific gravity of 3.68. The fluorescence reaction was strong orange in long-wave ultraviolet light and medium blue in short-wave UV (figure 2). The benitoite was slightly color-zoned orange and blue; the blue portion's pleochroism was very light blue and darker blue, while the orange portion's pleochroism was orangy yellow and dark orange. Microscopic examination showed altered crystals with discoid fractures (figure 3) and strong doubling. The discoid fractures were consistent with heated benitoite.

Benitoite is a barium titanium silicate ($\text{BaTiSi}_3\text{O}_9$) known as the California state gem, and it only occurs in gem quality in San Benito County, California. The New Idria District produces medium to medium-dark blue and lighter blue colors. According to a previous study published in *G&G*, pink and colorless examples are considered rare. In addition, heat treatment of lighter-color or colorless benitoite may result in an orange color. Since only a small portion of



Figure 1. The size and bright color of this 2.29 ct orange benitoite are exceptionally rare.

the treated material successfully changes color, orange benitoite is considered rare (B.M. Laurs et al., "Benitoite from the New Idria District, San Benito County, California," Fall 1997 *G&G*, pp. 166–187).

Figure 2. The orange benitoite's response to long-wave (left) and short-wave UV (right).

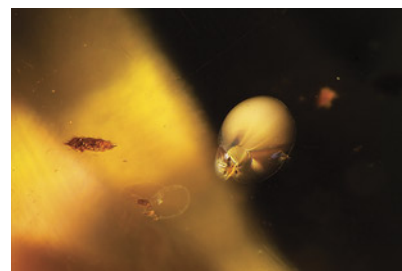
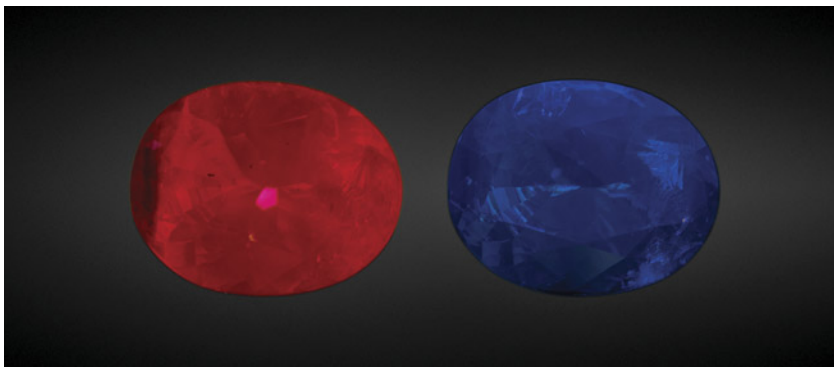


Figure 3. The orange benitoite contained several discoid fractures with healed fringes, consistent with heat-treated benitoite. Field of view 2.33 mm.

This benitoite was faceted by Bill Vance of Vance Gems, who stated that the rough was colorless prior to heat treatment. The bright orange color and large size make this an exceptional example of orange benitoite. Very few of these have been examined at GIA, and this 2.29 ct gemstone is the largest example we have observed.

Amy Cooper and Nathan Renfro

Editors' note: All items were written by staff members of GIA laboratories.

GEMS & GEMOLOGY, Vol. 58, No. 2, pp. 214–225.

© 2022 Gemological Institute of America



Figure 4. This set consists of a 48.63 ct piece of manmade glass (left), 9.17 and 6.21 ct laboratory-grown sapphires with resin imitation of matrix on the surface (center), and an 8.46 ct natural blue sapphire rough (right).

Interesting Set of BLUE “ROUGH” GEMSTONES

The selling of simulants and synthetics mixed with parcels of natural stones is an old form of deception. It usually happens close to mines, where inexperienced buyers assume the gemstones come directly from the source—and where advanced testing is likely not available prior to the purchase.

The Carlsbad laboratory recently received a group of four blue rough

stones (figure 4) submitted as natural sapphire for identification and origin reports. The largest weighed 48.63 ct and measured approximately $22.88 \times 19.67 \times 15.19$ mm. The material was partially fashioned, with evidence of polish lines on the surfaces. Careful microscopic examination revealed multiple gas bubbles, distinct flow marks associated with blue coloration, and conchoidal fractures. Weak snake pattern bands were observed under the polariscope. The hydrostatic specific

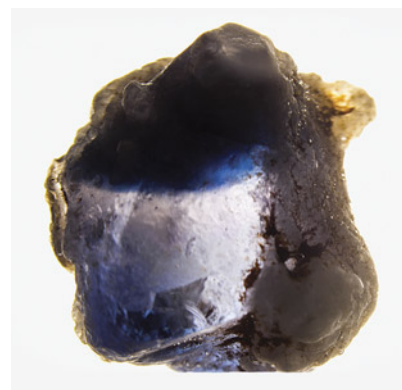
gravity was 2.48. These observations suggested a glass imitation, which was confirmed by comparing the infrared spectrum with that of manmade glass.

The next two were more convincing imitations of natural sapphire. They weighed 9.17 and 6.21 ct and measured approximately $16.00 \times 10.06 \times 8.30$ mm and $10.31 \times 9.38 \times 8.71$ mm, respectively. Resin that coated the surface (figure 5) resembled matrix composed of natural minerals commonly seen on natural corundum rough. The resin started to melt with the touch of a hot pointer. Brownish materials trapped in cavities resembled iron oxide stains one would expect to see in natural rough. Though difficult to see inside of the stones due to their rough surfaces, a few gas bubbles were observed through a small transparent area. Raman spectroscopy matched corundum, and immersion in water (figure 6) revealed curved blue banding. Laser ablation–inductively coupled plasma–mass spectrometry (LA-ICP-MS) detected no gallium and revealed trace elements of impurities consistent with synthetic corundum. Hydrostatic specific gravity values were 3.76 and 3.59, respectively. Both values were below the SG of corundum (3.9–4.05), a result of the lower SG of the resin on the surface. Both were reported as laboratory-grown sapphire with a comment stating, “Imitation matrix and resin is present on the surface.”

Figure 5. A resin imitation of matrix on the surface of a laboratory-grown sapphire. Field of view 7.19 mm.



Figure 6. Curved blue banding visible in the 6.21 ct laboratory-grown sapphire immersed in water.



The last piece of rough was a blue stone weighing 8.46 ct and measuring $13.85 \times 9.89 \times 7.60$ mm. The frosted natural surface made it difficult to see inside the stone, but some natural-looking fingerprints and strong, straight inky blue banding were observed. The Raman spectrum matched with corundum, and a hydrostatic SG of 3.96 confirmed it. The stone was immersed in methylene iodide to confirm the zoning was straight and not curved. Medium chalky blue fluorescence to short-wave UV and a strong 3309 cm^{-1} series in its Fourier-transform infrared (FTIR) spectrum proved that heat treatment had been applied to the stone. LA-ICP-MS revealed natural chemistry, including about 200 ppma iron and other trace elements such as gallium (~25 ppma), vanadium (~3.5 ppma), magnesium (~35 ppma), chromium (~1.5 ppma), and titanium (~80 ppma). Based on appearance, color zoning, and chemistry, this stone was reported as natural sapphire, heat treated, with Madagascar as the country of origin.

This was an interesting study of how synthetics and simulants can be mixed with their natural counterparts to misrepresent a parcel. However, careful examination and standard gemological testing are usually enough to identify them correctly.

Najmeh Anjomani

DIAMONDS

The Type IIb De Beers Cullinan Blue Diamond

Type IIb blue diamonds are extremely rare in nature. When people think of blue diamonds, the Hope diamond immediately springs to mind. The famed 45.52 ct Fancy Deep grayish blue cushion-cut treasure, now housed in the Smithsonian National Museum of Natural History in Washington, DC, has a long and fascinating history. First examined by GIA in 1960 and graded by GIA in 1988 (R. Crowningshield, "Grading the Hope diamond," Summer 1989 *G&G*, pp. 91–94), it



Figure 7. The 15.10 ct De Beers Cullinan Blue diamond.

shares many special gemological characteristics with other rare type IIb (boron-containing) diamonds such as the Wittelsbach-Graff, once assumed to be cut from the same rough crystal as the Hope. Here we report another special diamond of this group.

Recently graded by GIA and the recipient of a special monograph report was a 15.10 ct ($17.47 \times 11.53 \times 7.94$ mm) Fancy Vivid blue cut-cornered rectangular step cut. Named the De Beers Cullinan Blue diamond (figure 7; see video at www.gia.edu/gems-gemology/summer-2022-lab-notes-de-beers-cullinan-blue), it was cut from a 39.34 ct rough type IIb diamond crystal mined by Petra from the Cullinan

(formerly Premier) mine in South Africa. Compared to the Hope and Wittelsbach-Graff, both of which were mined in the Golconda region of India, the De Beers Cullinan Blue has some important similarities in gemological and spectroscopic features but shows clear variations. Natural type IIb blue diamonds over 10 carats are exceedingly rare.

The blue color is distributed evenly throughout the stone. Visual observation under a gem microscope revealed a very clean stone. No inclusions or graining were observed. Accordingly, the diamond received a clarity grade of Internally Flawless. Under conventional long-wave and short-wave UV radiation, it showed no observable fluorescence or phosphorescence. This feature is dramatically different from that of the Hope and Wittelsbach-Graff, two large type IIb blue diamonds that exhibit strong and prolonged red phosphorescence to conventional short-wave UV radiation.

The absorption spectrum in the mid-infrared region showed typical absorption features related to boron in diamond, such as strong absorption at $\sim 2800\text{ cm}^{-1}$ and a weak absorption peak in the range of $1332\text{--}1200\text{ cm}^{-1}$ (figure 8). The intensities of these absorptions indicated a high

Figure 8. The mid-infrared spectrum of the type IIb De Beers Cullinan Blue diamond.

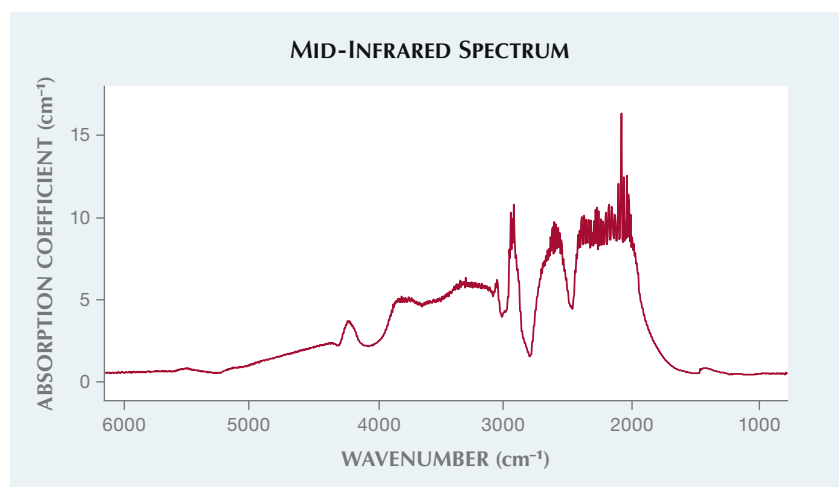


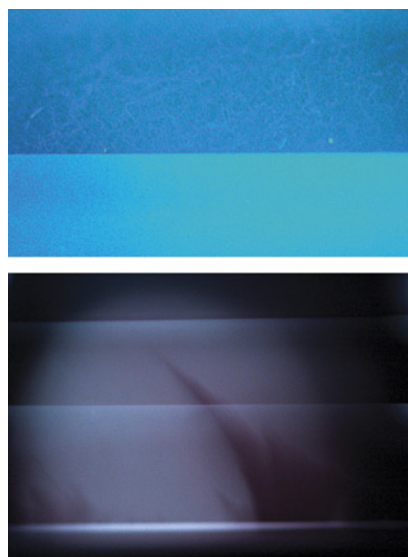


Figure 9. Observed with cross-polarized light was a strong tatami strain pattern with a dark gray color.

concentration of uncompensated boron of ~0.33 ppm. Natural type IIb diamonds typically contain 0.24–0.36 ppm (E. Gaillou et al., “Study of the Blue Moon diamond,” *Winter 2014 G&G*, pp. 280–286). The diamond’s boron concentration is close to that of the Hope (~0.36 ppm) and higher than that of the Wittelsbach-Graff (~0.19 ppm). Absorption from boron is the main contributor of color in natural type IIb diamonds.

Observation with a gemological

Figure 10. Under very strong short-wave UV, a weak aqua blue fluorescence with a subtle network of dislocations was observed (top). After exposure, a weak pinkish red phosphorescence was observed (bottom).



microscope equipped with crossed polarizers revealed a clear tatami pattern with a dark gray color (figure 9). Both the Wittelsbach-Graff and the Hope have different patterns and higher interference colors, a good indication that the De Beers Cullinan Blue has a much less distorted lattice structure. Under very strong short-wave UV, this diamond showed a weak aqua blue fluorescence with a subtle network of dislocations in the crystal structure, a pattern clearly different from the tight mosaic patterns observed in the Hope and the Wittelsbach-Graff (figure 10) (Gaillou et al., 2014).

These blue diamonds are among the rarest of gems. Recent research (E. Smith et al., “Blue boron-bearing diamonds from Earth’s lower mantle,” *Nature*, Vol. 560, No. 7716, 2018, pp. 84–87) has demonstrated that their boron derived from pieces of the earth’s crust sinking to the extremely deep depths of diamond formation. The gemological characteristics of the De Beers Cullinan Blue suggest it is one of these superdeep diamonds. Its combination of Fancy Vivid blue color grade in a step cut (a cut that does not enhance color, unlike other faceting

styles) (see video), 15.10 ct weight, and Internally Flawless clarity grade is exceptionally rare. It will remain one of the world’s most important diamonds.

Paul Johnson, A’Dhi Lall, Madelyn Dragone, and Stephanie Persaud

The Grass Is Always Greener...

The Carlsbad laboratory recently examined a 0.97 ct Fancy grayish green diamond submitted for colored diamond grading service. Microscopic examination revealed a colorless diamond with green radiation stains scattered across the pavilion (figure 11).

These radiation stains were particularly unusual due to their linear appearance and resembled blades of grass in their morphology and color. These stains were prevalent along intentionally preserved rough natural diamond surfaces on the pavilion. Faceted surfaces along the pavilion were polished with particular effort to retain some of the green radiation stains. The resultant internal reflection of green light to the table created a uniform green bodycolor in this rare and beautiful diamond.

Figure 11. Blade-like green radiation stains. Also indicated is the boundary of the close-up view of the green stains in figure 12. Field of view 2.9 mm.



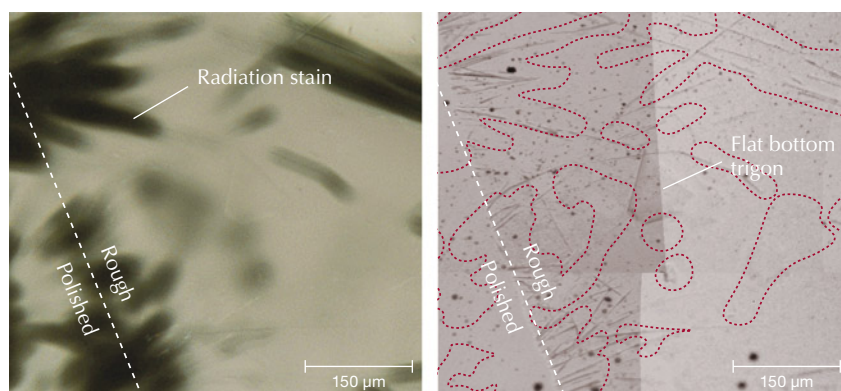


Figure 12. Radiation stains on the rough diamond's surface also penetrate to a polished side (left). Viewed with reflected light, the surface shows acicular indentations coincident with green stains (right).

Surface photomicrographs revealed long, linear, and acicular indentations concentrated near the center of the radiation stains (figure 12). Indentations crosscut flat-bottomed trigons, suggesting they post-dated diamond dissolution in the earth's mantle (e.g., R. Tappert and M. Tappert, *Diamonds in Nature: A Guide to Rough Diamonds*, Springer, Heidelberg, 2011). The green stains along the polished surface indicate that the radiation stains penetrated some depth into the diamond. These features have been observed previously at GIA (e.g., Spring 2021 *G&G Micro-World*, pp. 66–67; Spring

2022 *G&G Micro-World*, pp. 64–65) and may result from acicular to tabular radioactive minerals precipitating directly on the diamond surface in a paleoplacer to recent alluvial environment (e.g., R. Lauf, *Mineralogy of Uranium and Thorium*, Schiffer Publishing, Ltd., Atglen, Pennsylvania, 2016). Radiation damage created vacancies in the diamond lattice, which absorb red light and reflect green light, resulting in the green color of the radiation stains. Uncharged or neutral vacancies produce a photoluminescence response near the 741 nm zero phonon line called the GR1 defect (e.g., J.E. Shigley and C.M. Breeding,

"Optical defects in diamond: A quick reference chart," Summer 2013 *G&G*, pp. 107–111). The GR1 defect area from photoluminescence spectra can be measured and mapped to indicate the spatial distribution of this defect coincident with the radiation stains (figure 13).

It is unusual to see green radiation stains of this shape that correspond with indentations on a diamond surface. These features could be a commonly overlooked characteristic of green diamonds.

Michaela Stephan, Roy Bassoo, and Lo Combs

10 ct HPHT-Treated CVD LABORATORY-GROWN DIAMOND

Recent years have seen several size milestones for faceted diamonds grown by chemical vapor deposition (CVD). In all the published reports that commented on treatment, these record-size CVD diamonds were indicated to be as-grown and with no indications of post-growth treatment (Winter 2016 Lab Notes, pp. 414–416; "IGI Hong Kong certifies largest CVD grown diamond to date," 2020, <https://www.igi.org/gemblog/igi-hong-kong-certifies-largest-cvd-grown-diamond-to-date/>; Spring 2022 Lab Notes, pp. 54–56). For other recent milestone CVD diamonds reported within the trade, we could not confirm whether they were as-grown or treated. At the time of publication, the current benchmark is a 30.18 ct H-color diamond reportedly grown by Ethereal Green Diamond (Rapaport News, June 12, 2022).

Against this backdrop, a notable 10.04 ct CVD-grown diamond (figure 14) was recently submitted to the Carlsbad laboratory for a laboratory-grown diamond report. This emerald-cut stone with G color and VS₂ clarity had several growth remnants, including a cloud of dark non-diamond carbon. As with all laboratory-grown diamonds, it underwent extensive testing including spectroscopy to verify its CVD origin. IR absorption spectroscopy identified it as

Figure 13. Left: Map of the integrated area beneath the GR1 defect peak of the radiation stains on the diamond surface, derived from photoluminescence spectroscopy. Right: Reflected light image of the surface showing radiation stains (outlined in red) coincident with acicular indentations. The measurements were taken with a 532 nm laser at 1 mW power, 25 µm confocal spot size, 5 µm step size, and 100 Hz.

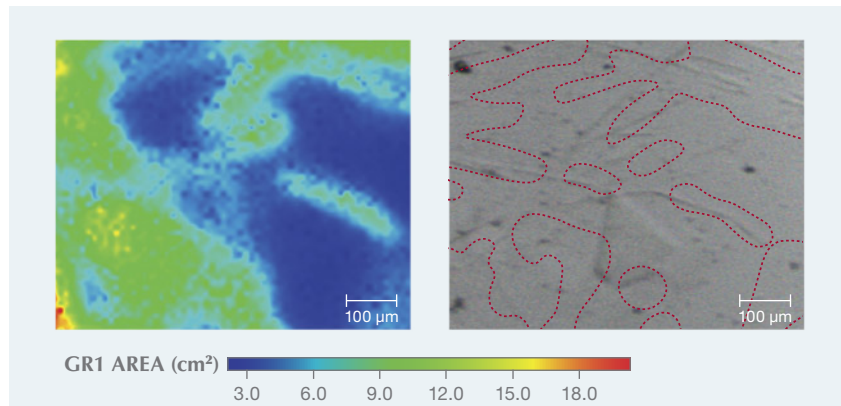
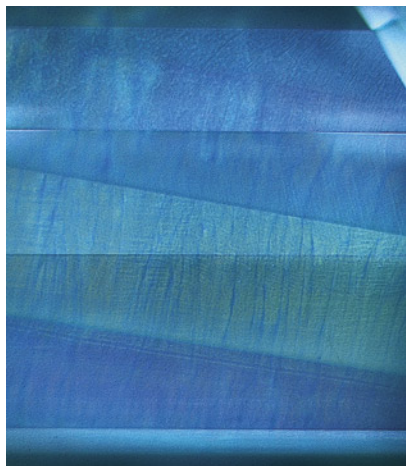




Figure 14. This 10.04 ct G-color CVD-grown diamond proved to have been HPHT treated.

type IIb with an uncompensated boron concentration of ~2 ppb. Spectral features such as the lack of a 468 nm peak in photoluminescence along with the coloration in the DiamondView fluorescence imaging (figure 15) confirmed it had undergone post-growth treatment (W. Wang et

Figure 15. The green and blue fluorescence colors in this DiamondView image confirm post-growth treatment of the 10.04 ct CVD-grown diamond.



al., "CVD synthetic diamonds from Gemesis Corp.," Summer 2012 *G&G*, pp. 80–97).

Many CVD-grown diamonds are subjected to high-pressure, high-temperature (HPHT) treatment after growth to remove a brownish appearance caused by extended defects (such as vacancy-related complexes). The brown color often correlates with a faster CVD growth rate, which the manufacturer uses knowing the color can be reduced by treatment afterward. It appears that when manufacturers create a CVD diamond of record-setting size, the growth is performed so slowly that subsequent HPHT treatment is not required for a colorless to near-colorless grade.

While some 80% of colorless to near-colorless CVD-grown diamonds have been subjected to post-growth treatment to reduce their brownish coloration (S. Eaton-Magaña et al., "Laboratory-grown diamond: A gemological laboratory perspective," *Jour-*

nal of Gems & Gemmology, Vol. 23, No. 6, 2021, pp. 25–39), this treatment is not often applied to larger stones. Therefore, evidence of HPHT treatment in a CVD-grown diamond larger than 10 carats is noteworthy. These products will likely become more commonplace in the future.

Sally Eaton-Magaña

PEARLS

A Reported Cassis Pearl from Key West, Florida

The Carlsbad laboratory recently examined an oval non-nacreous pearl weighing 29.78 ct and measuring 17.86 × 15.64 × 14.58 mm (figure 16). The pearl possessed a uniform pinkish orange bodycolor and a porcelainous surface with flame structures. The flames were short and wide and tapered to a point. This fine, well-formed flame structure looked like a homogeneous spotted pattern throughout the pearl's

Figure 16. This oval pinkish orange porcelainous pearl weighing 29.78 ct and measuring 17.86 × 15.64 × 14.58 mm was reportedly found in a queen helmet conch (*Cassis madagascariensis*), shown on the left with various *Cassis* species shells. Shells courtesy of Robin Willis.



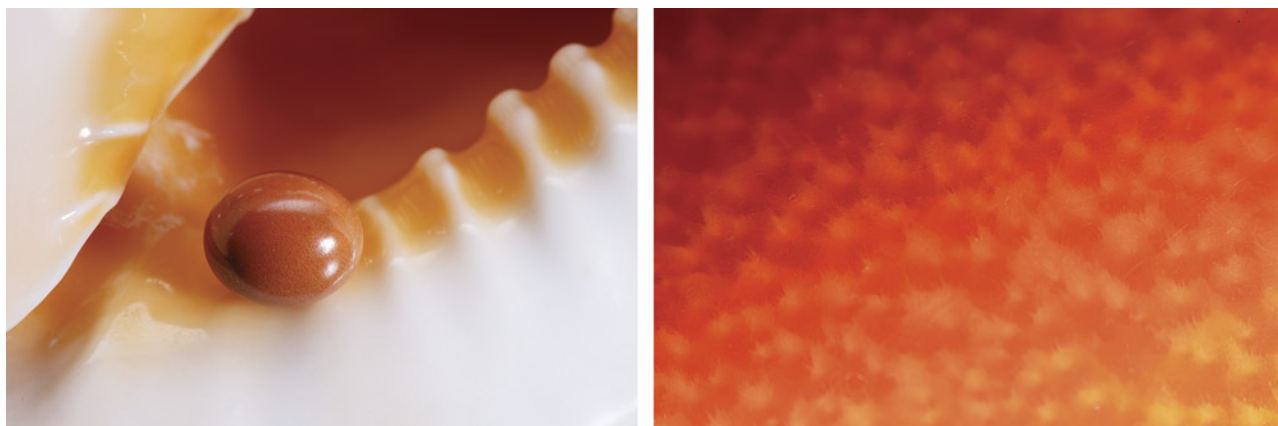


Figure 17. Left: This porcelainous pearl exhibited a fine, well-formed flame structure covering the entire surface, and a homogeneously spotted pattern was visible with the unaided eye. Right: Under magnification with fiber-optic illumination, the wide and spiky flame structure was evident. Field of view 2.90 mm.

surface (figure 17, left), yet the flame forms were evident at high magnification under the microscope (figure 17, right). Subsequently, Raman spectroscopic analysis with a 514 nm argon-ion laser verified the pearl was composed of aragonite, with peaks at 154, 181, 192, 207, 704, and 1085 cm^{-1} (J. Urmos et al., "Characterization of some biogenic carbonates with Raman spectroscopy," *American Mineralogist*, Vol. 76, 1991, pp. 641–646); two strong polyene peaks at 1131 and 1523 cm^{-1} were indicative of natural color (C. Hedegaard et al., "Molluscan shell pigments: An in situ resonance Raman

study," *Journal of Molluscan Studies*, Vol. 72, No. 2, 2006, pp. 157–162). Real-time microradiography (RTX) revealed a dark gray oval void-like feature in the center and a growth ring in the outer area of the pearl (figure 18). Such a void can be found in natural pearls from a number of porcelainous pearl-producing mollusks.

Orange porcelainous pearls are produced from various marine gastro-

pod species such as queen conch (*Lobatus gigas*), *Melo* species, *Cassis* species, and horse conch (*Fasciolarinae* subfamily). The flame characteristics and pinkish orange bodycolor of this pearl were unlike those of orange porcelainous pearls previously submitted to GIA. The client who submitted the pearl stated that it was found inside a queen helmet conch in the early 1960s by Bert Matcovich (fig-

Figure 18. RTX imaging revealed the growth structure of the pearl: an ovalish void-like feature of less radiopacity in the center and a growth ring in the outer area.

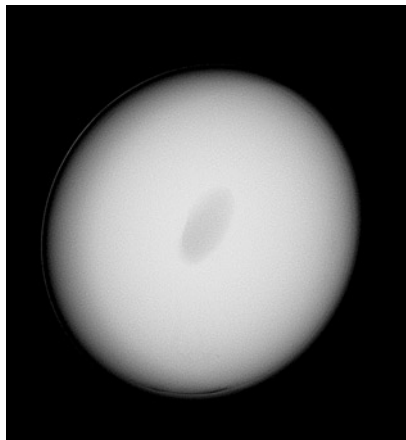


Figure 19. This photo shows the pearl and the queen helmet shell in which it was found. Photo courtesy of the Bert Matcovich family.



ure 19), who owned a shell shop in Key West, Florida. Born into a family of shellers with more than 60 years of experience, Matcovich fished the waters off Key West for conchs and visited local shrimp boats daily in the 1960s to purchase various types of shells. This pearl was a remarkable discovery.

Queen helmet, also known as emperor helmet, is the common name for a marine gastropod species called *Cassis madagascariensis*, which belongs to the Cassidae family. The species is generally distributed in the tropical western Atlantic, including the Caribbean Sea (J.H. Leal, "Gastropods," in K.E. Carpenter, *The Living Marine Resources of the Western Central Atlantic*, Vol. 1, Rome: Food and agriculture organization of the United Nations, 2002, pp. 99–127). Queen helmet shells have large, thick whorls with short spires, and three rows of knobs often appear on the body. They have a flat large parietal shield next to an aperture, and the color ranges from pale cream to deep salmon, often with a dark orangy brown color between the "teeth" (see again figure 19). Owing to their significant thickness, these colorful shells are widely used for cameo carving.

Cassis pearls typically have a fine and slender flame structure, often with intersecting flames. Their colors traditionally range from light orange to orangy brown, sometimes with patchy color. This pearl was unlike typical *Cassis* pearls examined by GIA, and its mollusk identity could not be confirmed with gemological testing. Nonetheless, this fine large natural non-nacreous pearl and its discovery story from six decades ago are noteworthy.

Artitaya Homkrajae, Michaela Stephan, and Amiroh Steen

RFID Device Embedded in South Sea Bead Cultured Pearl Necklaces

New technologies are increasingly being applied to cultured pearls, and it is exciting to witness developments in pearl traceability. GIA's Bangkok laboratory recently received two

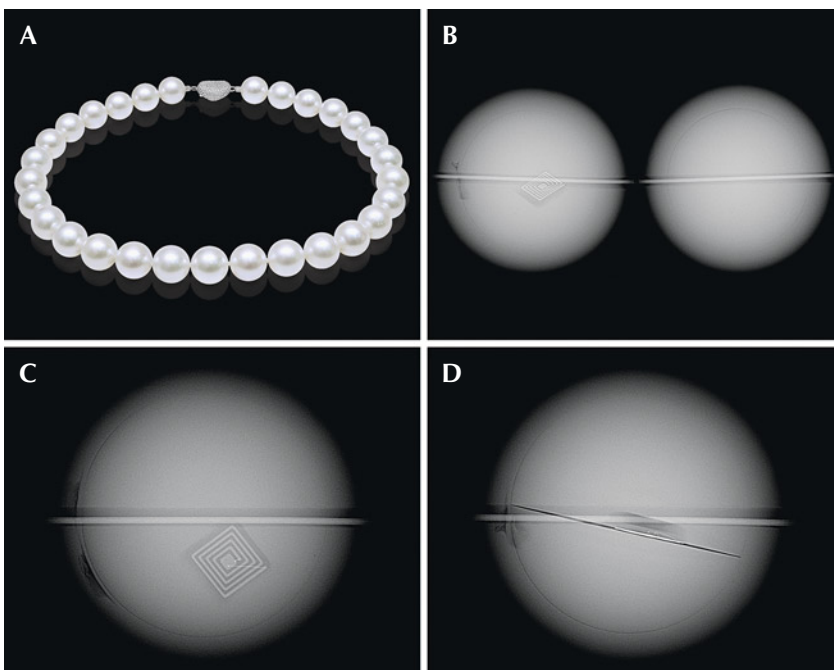


Figure 20. A: Necklace of South Sea bead cultured pearls, 14.80–15.90 mm in diameter. B and C: Real-time microradiography (RTX) revealed one bead cultured pearl in the necklace containing an RFID device showing an obvious demarcation of typical shell bead nuclei. The embedded electronic component is visible as a white opaque stepped square feature. D: When aligned at right angles to the previous direction, the electronic component is harder to see but can be observed within a long, sharp laminated plane separating the two parts of the shell bead nucleus.

South Sea bead cultured pearl necklaces, each consisting of 29 pearls ranging from 14.80 to 15.90 mm in diameter (strand A, figure 20A) and 14.40 × 14.20 mm to 16.20 mm in diameter (strand B, figure 21A). General observation under a binocular microscope revealed clear aragonite platelets characteristic of nacreous pearls, with no indications of treatment.

Real-time microradiography (RTX) revealed obvious demarcation features separating the shell bead nucleus from the overlying nacre layers. The nacre thickness range was consistent with bead cultured pearls produced by the *Pinctada maxima* mollusk (N. Sturman et al., "Bead cultured and non-bead cultured pearls from Lombok, Indonesia," Fall 2016 *G&G*, pp. 288–297). However, the most striking feature was the presence of some

electronic components within a few of the pearls. They were visible as opaque white squares with a stepped pattern in keeping with previously examined samples containing radio-frequency identification (RFID) devices (H.A. Hänni and L.E. Cartier, "Tracing cultured pearls from farm to consumer: A review of potential methods and solutions," *Journal of Gemmology*, Vol. 33, No. 7-8, 2013, pp. 239–246; Spring 2020 Lab Notes, pp. 134–136). Interestingly, only a single pearl in strand A (figure 20, B–D) and five pearls in strand B (figure 21, B–D) contained an RFID device. The device is usually positioned off the center of the bead to avoid being drilled.

GIA's Hong Kong lab has also begun seeing similar features in recent submissions (figure 22, A–B). The team compared the RTX data with

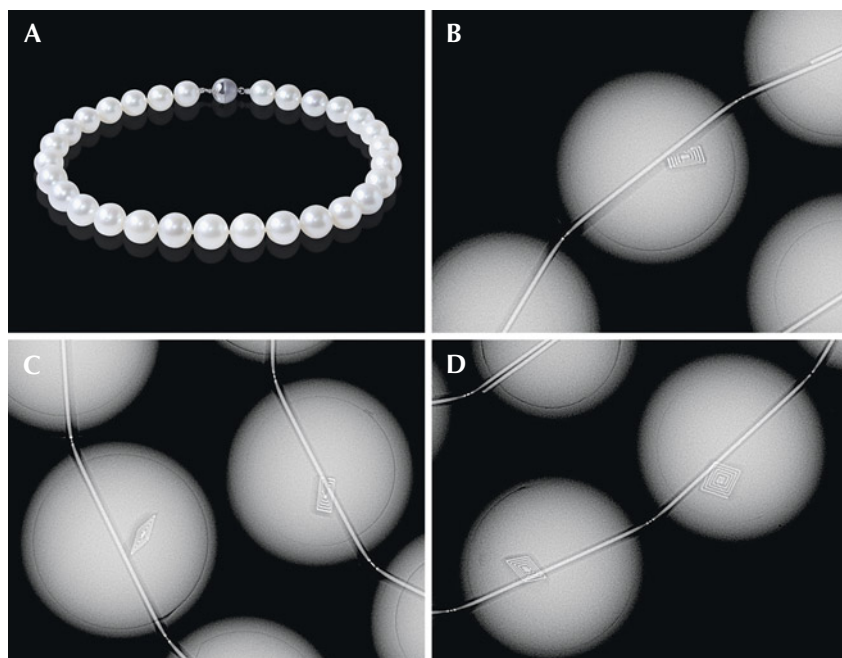
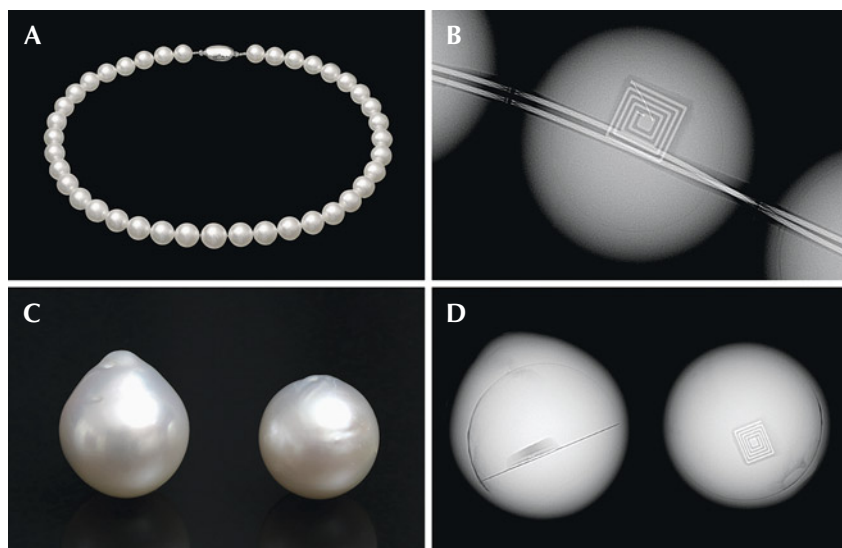


Figure 21. A: Necklace of South Sea bead cultured pearls, 14.40 × 14.20 mm to 16.20 mm in diameter. B–D: RTX analysis revealed five bead cultured pearls containing an off-center RFID device within the shell bead nucleus.

some known bead cultured pearls containing an RFID device (figure 22,

C–D) and confirmed that they were identical. The previous studies men-

Figure 22. A: Necklace of South Sea bead cultured pearls, 10.04–12.21 mm in diameter. B: RTX analysis of one of the pearls in the necklace revealed an RFID device. C: The internal structure was compared with two known bead cultured pearls containing RFID devices from GIA Hong Kong's reference collection, and they proved to be identical. D: RTX clearly showed the outline of the square RFID device, as well as the sawn plane and small recess where the RFID device had been placed.



tioned earlier describing RFID devices in bead cultured pearls have shown that these nuclei are produced by a patented pearl technology invented by Fukui Shell Nucleus Factory, which also supplies laminated beads to certain pearl farms. This explains the link between the laminating technique and its application in the production of RFID shell beads.

The use of RFID shell beads is known to assist in the storage of certain data such as a pearl farm's location, mollusk data, and harvest date. However, a specific RFID reader is required to retrieve the data, so we were unable to obtain the information stored within these particular devices. Since the RFID devices do not influence their external appearance, the pearls containing a shell bead nucleus with such components are still identified as bead cultured pearls. Because the RFID device could increase the weight and have a misleading effect if undetected, a special comment is routinely included on GIA pearl identification reports as a means of disclosure. While pearl tracing technology has not been extensively adopted by the cultured pearl industry, the increasing number of electronic devices in shell bead nuclei submitted to the laboratory is noteworthy. GIA will continue to monitor and provide updates to the pearl trade and consumers.

Nanthaporn Nilpetploy and
Ying Wai Au

Combination of Phenomena in Star and Cat's-Eye Color-Change SAPPHIRE

The Tokyo lab recently examined a transparent 20.49 ct violet to purple color-change double cabochon sapphire, measuring 16.67 × 14.69 × 8.51 mm (figure 23) with a specific gravity of 3.99 and a spot refractive index of 1.77. Usually a star sapphire is only polished on one side, and the unpolished side does not show any phenomena. But this stone was polished on both sides, which resulted in a unique



Figure 23. This 20.49 ct star sapphire with a combination of phenomena exhibited a color change from violet (top) to purple (bottom). Side A is shown in these photos.

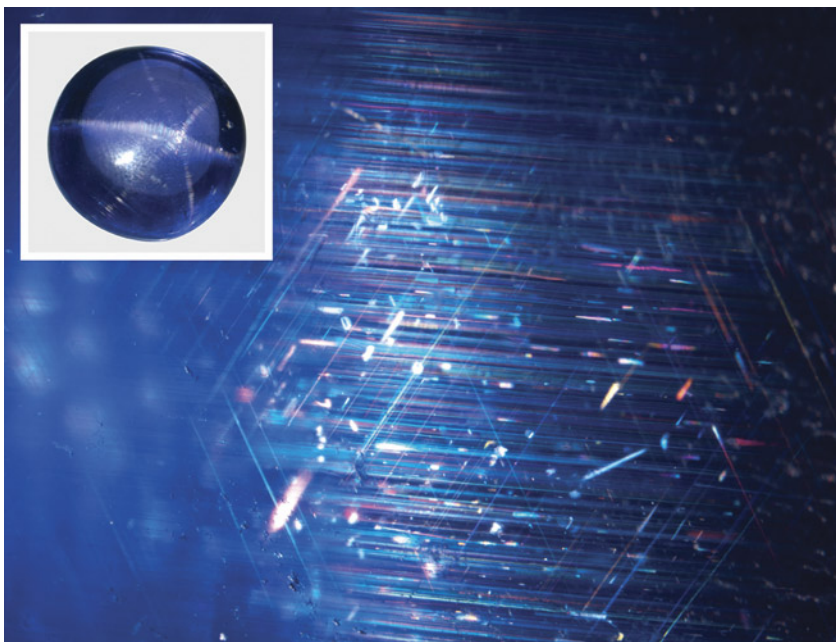
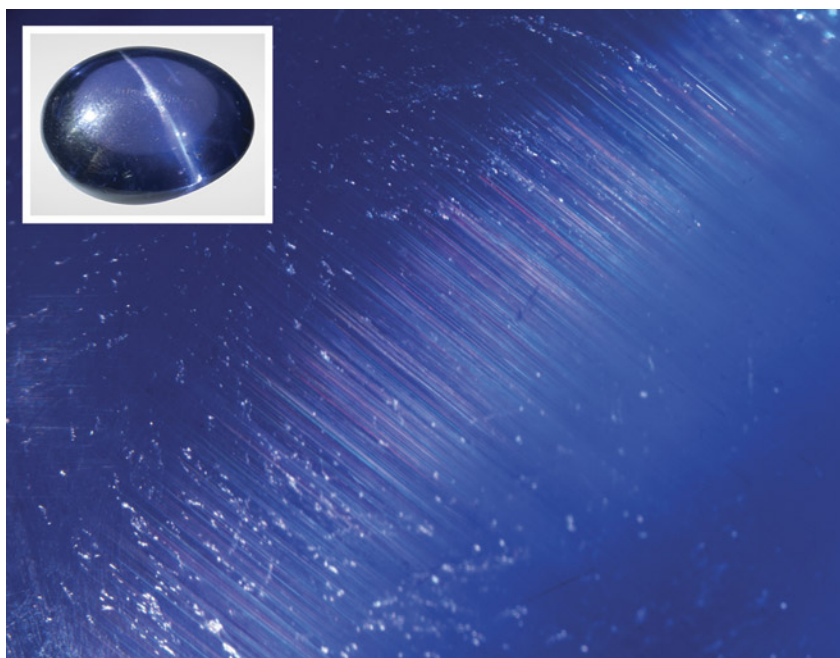


Figure 24. Side A: Intersecting sets of parallel needle inclusions producing six-rayed asterism. Field of view 5.8 mm. The photomicrograph is not aligned with the inset.

combination of phenomena. Side A displayed a six-rayed star. Side B also displayed a six-rayed star, but one line

containing two of the rays was much stronger, which made the phenomenon reminiscent of a cat's-eye.

Figure 25. Side B: Set of parallel needle inclusions producing chatoyancy. Field of view 5.8 mm. The photomicrograph is not aligned with the inset.



Chatoyancy is displayed when light reflects off a set of dense parallel elongated inclusions, such as needles; asterism occurs when such a set of inclusions is oriented in multiple directions. In the case of this stone, side A with the distinct six-rayed star had three sets of dense parallel needles and platelets close to the surface, intersecting at 60° angles (figure 24), which is common with six-rayed asterism. Side B also had three sets of these needles close to the surface, but the needles were more concentrated in one of the directions, producing a cat's-eye effect (figures 24 and 25). Interestingly, the chatoyancy in Side B and one line of asterism in Side A are contributed by the same group of needles.

Although color-change star sapphire is not particularly rare, color-change cat's-eye sapphire is far less common. Color-change sapphire with asterism on one side and chatoyancy on the other is without question a "phenomenal" gem.

Masumi Saito and
Yusuke Katsurada

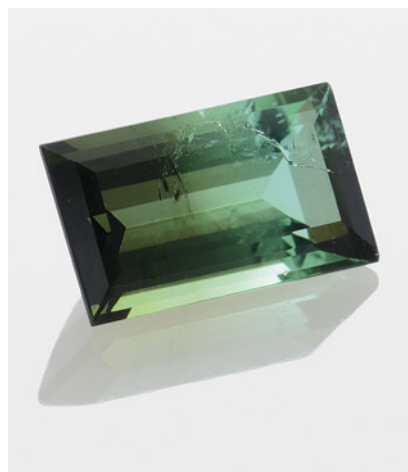


Figure 26. The 1.62 ct bicolor copper-bearing tourmaline.

TABLE 1. Mn, Fe, and Cu concentrations on each side of the bicolor tourmaline, measured by LA-ICP-MS (in ppmw, average of three spots).

	Mn	Fe	Cu
Bluish green	22826	566	7850
Dark yellowish green	17233	11287	4953
Detection limit (ppmw)	7.13	3.10	0.11

Bicolor Cuprian TOURMALINE

A bicolor gem has two colors in one stone. Ametrine is a well-known bicolor gem, a purple and yellow quartz combining amethyst and citrine. In

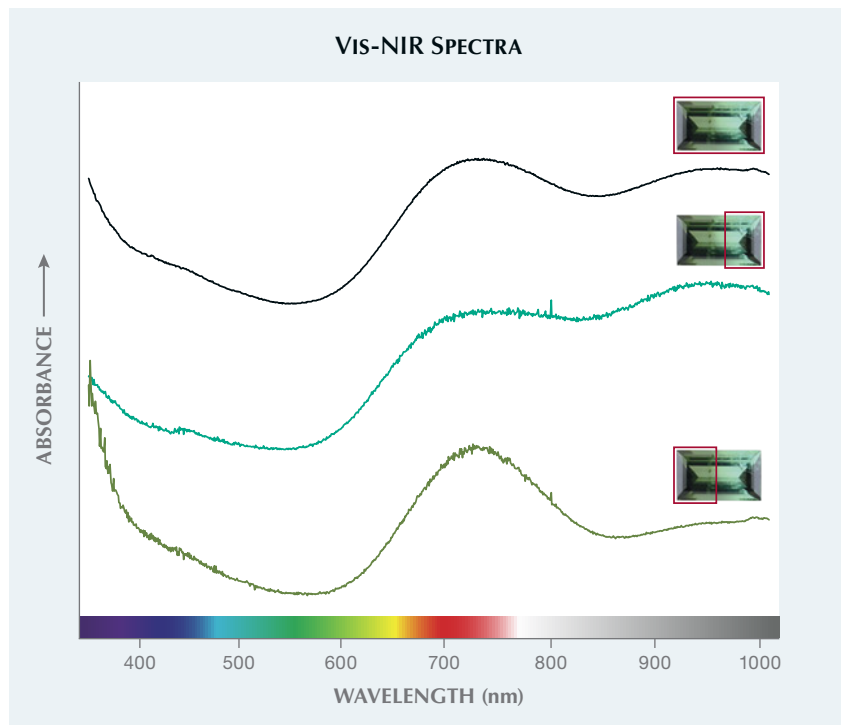
addition to the ametrine variety of quartz, other colored gemstones such as corundum and tourmaline can be naturally bicolor, although most of them do not have a specific variety

name. Most bicolor gem materials are cut to show different colors that are obvious when viewed in face-up orientation.

The Tokyo laboratory recently examined a bicolor rectangular step cut weighing 1.62 ct and measuring $9.14 \times 5.47 \times 3.71$ mm (figure 26). The color was gradually distributed from bluish green to dark yellowish green along the length. This stone was doubly refractive with a refractive index of 1.620–1.640 and a specific gravity of 3.10. Microscopic observation revealed networked fluid inclusions and strong doubling. The stone was identified as tourmaline by these gemological features.

Paraíba tourmaline, a certain type of copper-bearing tourmaline, has been one of the most sought-after gemstones in the trade over the last three decades. In 2012, the Laboratory Manual Harmonisation Committee (LMHC) updated the definition of Paraíba tourmaline as “a blue (electric blue, neon blue, violet blue), bluish green to greenish blue, green (or yellowish green) tourmaline of medium-light to high saturation and tone (relative to this variety of tourmaline), mainly due to the presence of copper and manganese.” Visible/near-infrared (Vis-NIR) absorption was collected with GIA’s custom-made UV-Vis spectrometer to determine the chromophore. To be considered Paraíba tourmaline, the copper-related absorp-

Figure 27. Vis-NIR absorbance of the whole tourmaline (top), the bluish green portion (middle), and the dark yellowish green portion (bottom). Copper absorption is in the red (approximately 730 nm) and near-infrared regions (approximately 980 nm). Iron absorption is only in the red region (approximately 730 nm). Spectra are stacked for clarity.



tion needs to be dominant and the color appearance should be within the defined range.

Non-polarized absorption spectra of the whole stone showed two bands in the red and near-infrared regions (figure 27, black line). To measure the spectra of each color separately, one half of the gem was covered with opaque black cardboard to allow light to pass through only one color at a time. The results indicated that the dominant chromophore was different (figure 27; bluish green and dark green lines at the middle and bottom, respectively)—the bluish green part is colored by copper, whereas the dark yellowish green part is colored by iron (P.B. Merkel and C.M. Breeding, "Spectral differentiation between copper and iron colorants in gem tourmalines," Summer 2009 *G&G*, pp. 112–119).

The trace element composition of each differently colored region was analyzed by laser ablation–inductively coupled plasma–mass spectrometry (LA-ICP-MS). As shown in table 1, the bluish green side shows lower iron (566 ppmw) and higher copper (7850 ppmw), and the dark yellowish green side shows higher iron (11287 ppmw) and lower copper (4953 ppmw). Comparing the different Vis-NIR absorption patterns of these portions (figure 27), the association of copper and iron for each color portion is in agreement with Merkel and Breeding (2009). By virtue of its color and its chromophore, only the bluish green portion is consistent with the definition of Paraíba tourmaline.

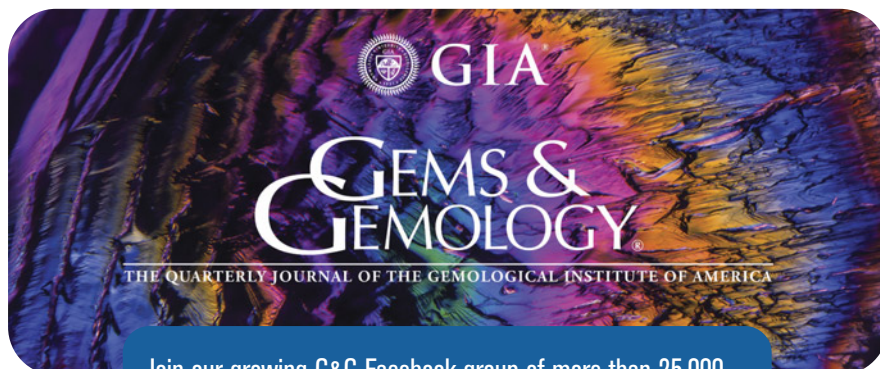
Sometimes we encounter cuprian tourmaline with chemical zoning, which has varying trace element concentrations within. A drastic differ-

ence, as in the case of this bicolor tourmaline with a non-Paraíba iron-colored portion, is not typical. The dark yellowish green part could have been polished off to make this a typical Paraíba tourmaline.

Yusuke Katsurada

PHOTO CREDITS

Nathan Renfro—1–3; Annie Haynes—4, 14; Najmeh Anjomani—5, 6; Towfiq Ahmed—7; Madelyn Dragone—9; Stephanie Persaud—10; Michaela Stephan—11, 12; Roy Bassoo—12; Taryn Linzmeyer—15; Robert Weldon—16, 17 (left); Artitaya Homkrajae—17 (right); Amiroh Steen—18; Nuttapol Kitdee—20A, 21A; Tony Leung—22A; Shunsuke Nagai—23; 24 (inset), 25 (inset), 26; Yusuke Katsurada—24, 25



The image shows the cover of the GIA GEMS & GEMOLOGY journal. The cover features a vibrant, abstract background with shades of purple, blue, and yellow. The GIA logo is prominently displayed at the top left, followed by the title "GEMS & GEMOLOGY" in large, stylized letters. Below the title, it reads "THE QUARTERLY JOURNAL OF THE GEMOLOGICAL INSTITUTE OF AMERICA". At the bottom, there is a blue banner with white text that says: "Join our growing G&G Facebook group of more than 25,000 members, connecting gem enthusiasts from all over the world!"

